# SCIENTIFIC REP🅞RTS

**OPEN**

# SIMcheck: a Toolbox for Successful Super-resolution Structured Illumination Microscopy

Graeme Ball[1,†], Justin Demmerle[1], Rainer Kaufmann[1,2], Ilan Davis[1], Ian M. Dobbie[1] & Lothar Schermelleh[1]

**Three-dimensional structured illumination microscopy (3D-SIM) is a versatile and accessible method for super-resolution fluorescence imaging, but generating high-quality data is challenging, particularly for non-specialist users. We present *SIMcheck*, a suite of ImageJ plugins enabling users to identify and avoid common problems with 3D-SIM data, and assess resolution and data quality through objective control parameters. Additionally, *SIMcheck* provides advanced calibration tools and utilities for common image processing tasks. This open-source software is applicable to all commercial and custom platforms, and will promote routine application of super-resolution SIM imaging in cell biology.**

The last decade has witnessed the spread of super-resolution light microscopy techniques that surpass the long-standing diffraction limit of optical resolution[1–3]. This has ushered in a second fluorescence microscopy revolution[4], enabling researchers to better assess the location, structure, and dynamics of specifically labelled macro-molecules, thus beginning to bridge the gap between light microscopy and structural biology. Linear two- or three-dimensional structured illumination microscopy (SIM, 3D-SIM) provides multicolour optical sectioning with double the conventional resolution in the lateral[5,6] and axial[7,8] dimensions allowing fast 3-dimensional imaging of fixed and live specimens[9–12]. This is achieved by moving high-frequency information into the observable range of the microscope by frequency mixing with a fine-striped pattern of illumination. By imaging variations of the phase and angle of the illumination pattern this information can be computationally separated and recombined to reconstruct a super-resolution image with twice the frequency support in two or three dimensions[13]. Currently, the best practice in acquisition and processing of SIM data requires considerable expertise[14,15] which represents a significant barrier to exploiting the full potential of SIM imaging[16]. Inaccurate instrument settings and suboptimal imaging conditions cause artifacts that are often difficult to distinguish from relevant structural features. Furthermore, there are no dedicated tools designed for thorough and unbiased quality assessment, and standardized post-processing of SIM data.

Here we describe *SIMcheck* (https://github.com/MicronOxford/SIMcheck and Supplementary Software), a user-friendly and simple solution to this challenge, which lowers the activation energy required for less experienced users and helps specialists and non-specialists to capture excellent quality 3D-SIM data and interpret it correctly. *SIMcheck* consists of a suite of plugins for the widely-used open-source application *ImageJ*[17]. It provides tools for assessment of the resolution, image quality and identification of sources of errors and artifacts in SIM imaging, as well as simplifying calibration and image handling steps. Additionally, *SIMcheck*'s output offers suggestions for how to address common deficiencies in SIM data. Raw and reconstructed data from any commercial SIM platform can be analysed with several options, and produce a variety of quality check outputs, a log text containing important metrics, and an output table with assessment of the data quality based on key statistics (Table 1,

[1]Department of Biochemistry, University of Oxford, Oxford, UK. [2]Division of Structural Biology, Wellcome Trust Centre for Human Genetics University of Oxford, Oxford, UK. [†]Present address: Dundee Imaging Facility, School of Life Sciences, University of Dundee, Dundee,UK. Correspondence and requests for materials should be addressed to L.S. (email: lothar.schermelleh@bioch.ox.ac.uk)

| | | Function Title | Window Title | Function | Output Type & Metrics | System Calibration | Acquisition Parameters | Recon. Parameters | Sample Preparation | Low Mod. Contrast | Image Processing | Figure |
|---|---|---|---|---|---|---|---|---|---|---|---|---|
| Raw data check | 1 | Channel Intensity Profiles | [Image]_CIP | Plots average intensity per image plane for each angle and z-position | • Average intensity decay (%)<br>• Maximum intensity difference per angle (%)<br>• Maximum intensity fluctuation per angle (%)<br>• Total Intensity Variation (TIV) per angle (%) | ✓ | ✓ | | | ✓ | | 1a,b S3 |
| | 2 | Fourier Projection | [Image]_FPJ | Z- and phase-projection of 2D FFTs over all angles | • Visual inspection of Fourier transform | ✓ | ✓ | | | ✓ | | 1c, S4 |
| | 3 | Motion & Illumination Variation | [Image]_MIV | Highlights image features that differ between acquisition angles | • Visual inspection of colour deviation<br>• Error per channel (%) | ✓ | | | ✓ | | | 1d, S5 |
| | 4 | Modulation Contrast | [Image]_MCN | Assesses the ratio of illumination stripe contrast to noise intensity per voxel | • Modulation contrast-to-noise ratio (MCNR)<br>• Visual inspection of image heatmap<br>• Average feature MCNR<br>• High-frequency noise filter recommendation | ✓ | | | ✓ | ✓ | | 1e, S6 |
| Reconstructed data check | 1 | Intensity Histogram | [Image]_RIH | Overlays linear- and log-scaled intensity histograms | • Max-to-min intensity ratios (MMR) (%)<br>• Max/min pixels (n)<br>• Visual inspection of histogram | | ✓ | ✓ | | | | 2b, S7 |
| | 2 | Spherical Aberration Mismatch | [Image]_SAM | Plots minimum and mean intensity in each z-plane, calculates standard deviation of minimum / mode | • Visual inspection of plot<br>• Z-minimum variation (ZMV) | ✓ | | ✓ | | | | 3e,f |
| | 3a | Fourier Plot - Lateral | [Image]_FTL | Displays FFT in XY for each z-plane | • Visual inspection of lateral Fourier transform plot | ✓ | | ✓ | | | | 2e-h, S9 |
| | 3b | Fourier Plot - Orthogonal | [Image]_FTO | Displays Y-projected FFT in XZ | • Visual inspection of orthogonal Fourier transform plot | ✓ | | ✓ | | | | 2e-h, S9 |
| | 3c | Fourier Plot - Radial | [Image]_FTR | Displays normalized integrated intensity over radius in reciprocal distance | • Visual inspection of graph | ✓ | | ✓ | | | | 2e-h, S8 |
| | 4 | Modulation Contrast Map | [Image]_MCM | Plots MCN data and heatmap on top of reconstructed data | • Modulation contrast-to-noise ratio (0–24)<br>• Visual inspection of image heatmap | | ✓ | ✓ | ✓ | ✓ | | 2d, S6 |
| Calibration | 1 | Illumination Pattern Focus | [Image]_IPF | Shows orthogonal view for first phase of each angle of raw data (bead lawn recommended) | • Visual inspection of illumination pattern | ✓ | | | | | | 3d, S10 |
| | 2 | Illumination Phase Steps | [Image]_IPS | Performs tests for stability and alignment of phases (bead lawn recommended) | • Standard deviation of illumination pattern frequency (n)<br>• Phase step size (radians)<br>• Phase step reproducibility (%)<br>• Visual inspection of Fourier transform | ✓ | | | | | | 3g, S10 |
| Utilities | 1 | Format Converter (Nikon/Zeiss to OMX) | [Image]_OMX | Converts Nikon (.nd2; tiled) or Zeiss (.czi; CZPAT) format files for further analyses | • OMX format (CPZAT) image (.dv). | | | | | | ✓ | S3 |
| | 2 | Raw SI to Pseudo-Widefield | [Image]_PWF | Averages phases and angles for comparison with reconstructed SIM image | • Widefield image (.tif) | | | | | | ✓ | 3b, S7 |
| | 3 | Threshold and 16-bit Conversion | [Image]_THR | From 32-bit reconstructed images, discards intensities below a threshold and fills 16-bit range | • 16-bit (.tif) image, default mode-thresholded, for downstream processing. | | | | | | ✓ | 3c, S7 |
| | 4 | Stack FFT | [Image]_FFT | Applies 2D FFT with a Gaussian window function to each z-plane | • Visual inspection of Fourier transform | ✓ | | | | ✓ | | 3f, S4 |

**Table 1. SIMcheck functionalities.** Each check is listed by: title; window title of the output; the main function of the check; and the expected output and metrics. The category to which each check or tool may apply is indicated by checkmarks. The corresponding Figures in the main text and Supplementary Information are listed, showing examples and containing more detailed instructions and explanations for each check respectively. Additional notes and interpretation guidelines are listed in Supplementary Table S2.

Supplementary Fig. S1). The names, function, type of output, areas of concern, and corresponding figures for each check are listed in Table 1. Corresponding log entries including interpretation guidelines are listed in Supplementary Table S2. A schematic representation summarizing how each check applies to the SIM imaging workflow is shown in Fig. 1, and the various functionalities of *SIMcheck* are colour-coded to correspond to the remaining figures.

### Structured illumination data checks

Raw SIM data (Fig. 2a), prior to reconstruction, can be used to diagnose problems from three sources: (1) system calibration; (2) acquisition practices; (3) sample preparation (Table 1, Fig. 1). Deficiencies in any of these areas can lead to substantial artifacts after reconstruction, compromising the resolution of the images and making misinterpretation of results more likely. Loss or strong variations of signal intensity and the associated drop in signal-to-noise-ratio (SNR) in the raw data during acquisition can have a profound effect on the reconstruction output. Thus, the first raw data check is a *Channel Intensity Profile* (Fig. 2b) providing a plot of the average intensity for each z-plane, visualizing the rate of bleaching, intensity fluctuations, and differences in intensity between illumination pattern angles. Summary statistics report numerical values for each, together with the combined total intensity variation (TIV) over a central window of 9 z-planes (= 135 images) (Supplementary Fig. S3).

To assess data quality in frequency space, the second check is a *Raw Fourier Projection* (Fig. 2c, Supplementary Fig. S4) of the entire z-stack. For samples that are sufficiently labelled and well contrasted, this allows the illumination pattern to be checked for clean first and second order spots, which represent high-frequency information (Fig. 2c, arrows). Raw data can also be viewed in reciprocal space for each individual image with the *Stack FFT* utility (Table 1, Supplementary Fig. S5).

The *Motion & Illumination Variation* check averages and intensity-normalizes the five phase-shifted images acquired for each plane for the different illumination pattern angles. It then assigns a false colour (cyan, magenta, yellow) to each angle (Fig. 2d). Subsequent merging of the angle information into one CMY image reveals intensity differences between temporally separated acquisitions as coloured sub-regions, whereas homogeneous data appears grey-white. This check can highlight uneven field-illumination or movement during acquisition, both of which can cause local reconstruction artifacts (Supplementary Fig. S5).

Intensity of the modulation contrast (or stripes) in the raw image is a key determinant of reconstructed image quality, as it critically affects the amount of frequency-shifted information that can be reassigned in the reconstruction process. Thus, the fourth check, *Raw Modulation Contrast* (Fig. 2e), calculates the ratio of the modulation contrast-to-noise (MCN) within the image by a specially devised Fourier analysis (Supplementary Fig. S6) and translates this to a heat map using a custom look-up-table (LUT). The check then reports an average modulation contrast-to-noise ratio (MCNR) for auto-segmented features and provides a recommended value for the high-frequency (Wiener) filter to be used for reconstruction (see **Methods**).

Analysis of reconstructed SIM data (Fig. 3) can diagnose problems that arise from system calibration errors, inappropriate acquisition settings, and from sub-optimal reconstruction parameters. The *Reconstructed Intensity Histogram* check (Fig. 3a,b) illustrates the proportion of pixel intensities above and below the mode (peak of the full-range histogram of the unprocessed image stack), and reports a minimum-to-maximum ratio (MMR) as a metric for the level of the feature intensity relative to reconstructed noise and intensity dips generated in the reconstruction process (Supplementary Fig. S7). Various factors can contribute to a low MMR, the most common being poor signal-to-noise and/or modulation contrast ratios in the raw data (e.g. by insufficient sample labelling, acquisition settings, or spherical aberration). Thus, the MMR serves as valuable indicator of the quality of reconstruction that can be used to diagnose various sources of error. Since the intensity values below the mode do not contain any feature information it is used as the default threshold for the *Threshold and 16-bit Conversion* utility (see below, Fig. 3c, Supplementary Fig. S7) and as an optional pre-processing step in the Fourier space analysis (below).

The reconstruction quality of specific structural features can vary in different regions of an image, and is dependent on variations in the underlying modulation contrast (e.g. by the local contribution of out-of-focus blur). To highlight these local variations, the *Modulation Contrast Map* check utilizes the MCN values from the *Raw Modulation Contrast* output to combine the colour look-up-table encoding the raw MCN values with the intensity information from the reconstructed data (Fig. 3d, Supplementary Fig. S9). Visual inspection allows assessment of how well the local modulation contrast in the raw data supports features observed in the reconstruction, with a very low level of underlying MCNR increasing the likelihood that an observed "feature" originates from reconstructed noise.

As with raw data, viewing reconstructed data in reciprocal space offers complementary information on image quality and resolution[18]. The *Reconstructed Fourier Plots* check contains three representations of the reconstructed data's Fourier transform, in the lateral and axial directions, and a radial profile plot of the central slice in the lateral Fourier transform (Fig. 3e–h, top middle and bottom panels, Supplementary Fig. S8), respectively. The effective resolution of the reconstruction may be estimated, and errors resulting in atypical patterns can be identified (Supplementary Fig. S9). The axial Fourier plot is generated from an orthogonal cross section of the reconstructed data (Fig. 3a), to determine the frequency support/resolution of a 3D reconstruction along the z-axis (Fig. 3e–h, Supplementary Fig. S8).
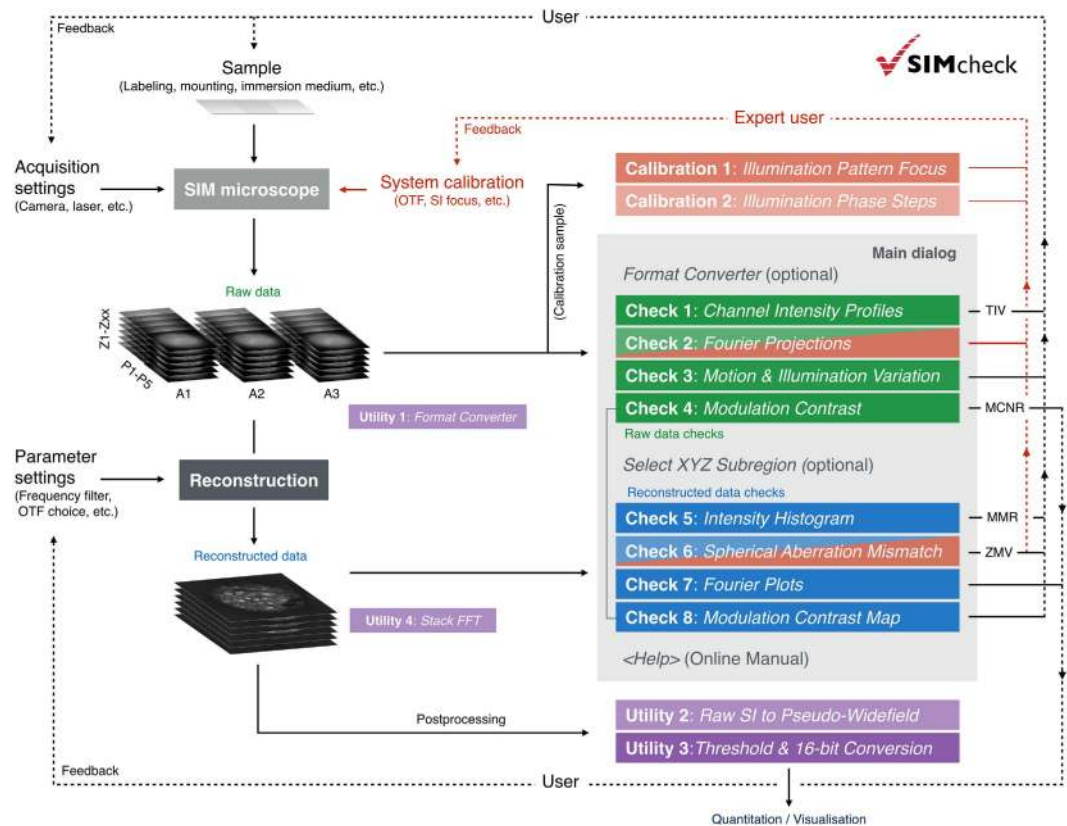
**Figure 1. Integration of SIMcheck functionalities to the SIM imaging workflow.** Solid lines represent the user's workflow, and point from the various workflow steps to the applicable functions of *SIMcheck*. Dashed lines represent where SIMcheck's output can inform user decisions, either in sample preparation, acquisition settings, reconstruction parameter settings, or system calibration. Colour codes are as follows: blue – raw data checks; green – reconstructed data checks; purple – utilities; red – applicable to expert users only.

Lastly, the *Spherical Aberration Mismatch* check plots the minimum values for each z-section in comparison to the mean feature intensity and reports the z-minimum variation (ZMV) as a metric for the "depth of intensity dips" relative to the average feature intensity (Fig. 4e–f). Strong intensity dips and prominent side lobes around brighter features ("echo signals"), as well as reduced overall intensity are a hallmark of mismatch between the real point spread conditions in the sample and the ideal system behaviour encoded in the optical transfer function (OTF), the Fourier transform of the point spread function that is used for the reconstruction. In practice, this artifact type is mostly caused by increased levels of spherical aberration in the sample through variations in depth, refractive indices, temperature, etc. In addition, shifting of the illumination pattern focus (see below) can have a similar effect, which may call for a recalibration of the system. The ZMV metric is most useful as a relative measure to compare the same or very similar samples under variable acquisition conditions or reconstruction settings (e.g. to compare refractive index variation or different OTFs). These eight checks compose the core of *SIMcheck*'s functionality for the routine user, and are recommended to validate data for each sample type in an imaging experiment (Fig. 1).

**System calibration tools and image processing utilities.** Additionally, *SIMcheck* contains two advanced system calibration tools, for use by imaging professionals to document system alignment, confirm system performance, and facilitate appropriate maintenance. Both tools require raw data containing an evenly covered field of sub-resolution fluorescent beads, or similar (Fig. 4a). The first of these checks is the *Illumination Pattern Focus*, which generates an orthogonal view of the illumination pattern for each illumination angle from the raw data (Fig. 4d, Supplementary Fig. S10). This can inform service of the instrument to ensure the highest intensity of modulation contrast at the image plane (Table 1). The second check analyses the *Illumination Phase Steps*, and reports on the reproducibility, and standard deviation of phase stepping for each illumination angle (Fig. 4g, Supplementary Fig. S10). This information allows for improved diagnostics, and can be an essential alignment tool for home-built or substantially modified instruments (Table 1).

Finally, *SIMcheck* contains a set of utilities to facilitate image handling and processing. The *Format Converter* takes data in .nd (Nikon) and .czi (Zeiss) file formats and reorders them into the default (GE
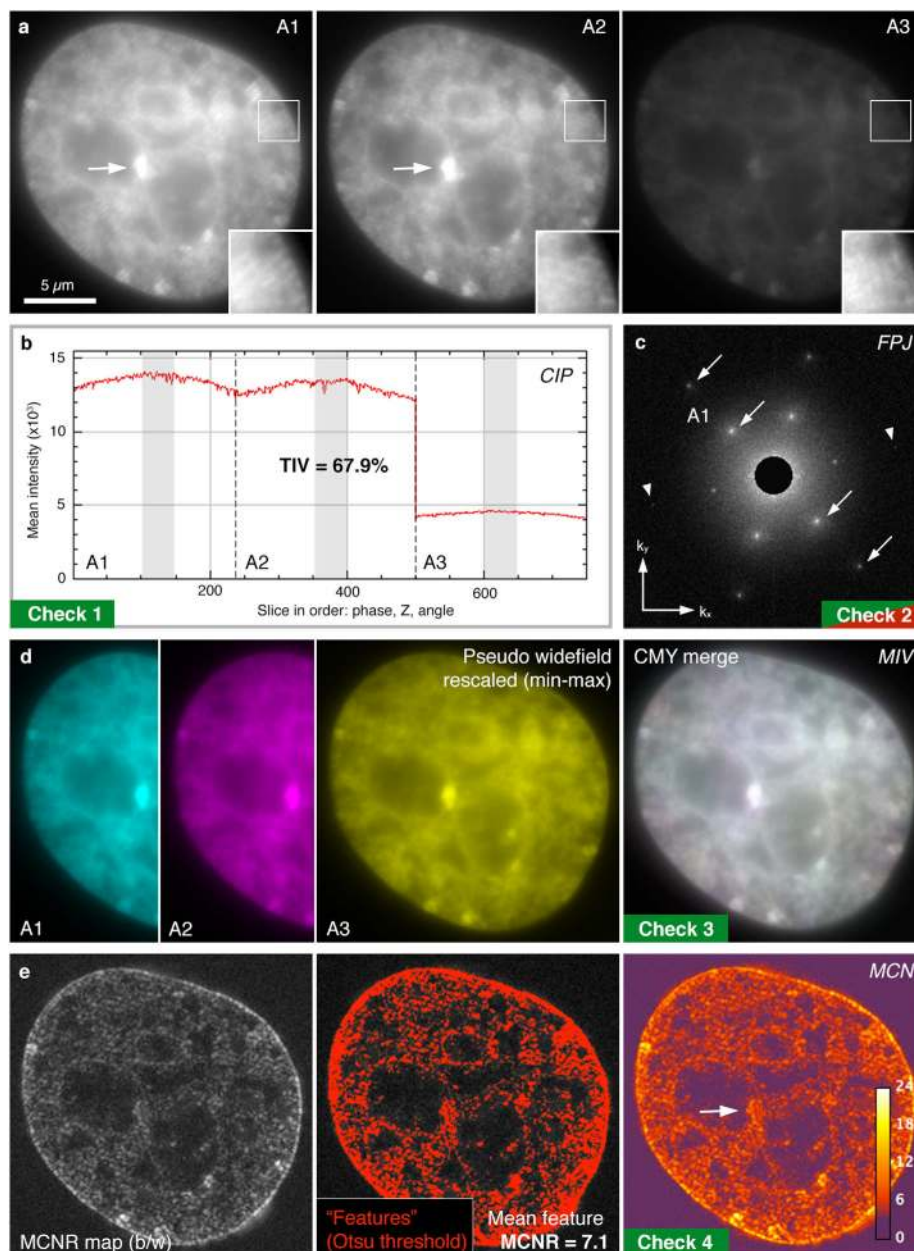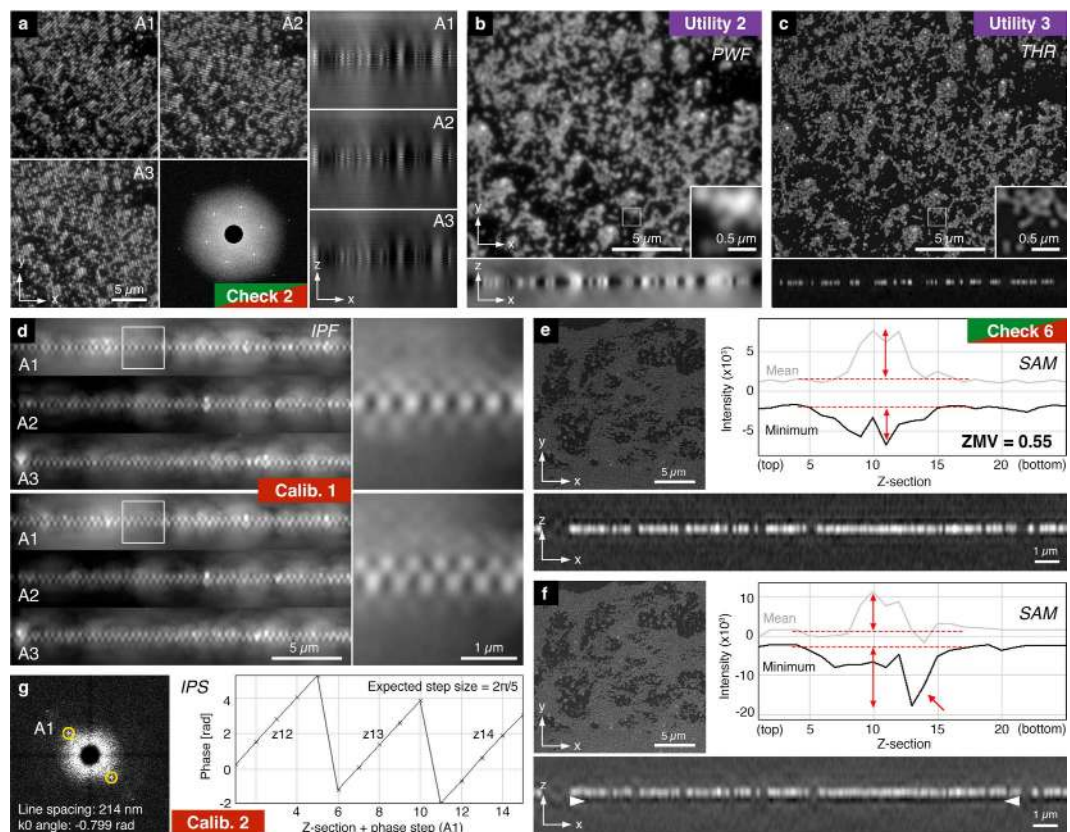
**Figure 2. SIMcheck output for raw SIM data**. (**a**) Representative images from a 3D-SIM dataset taken from a DAPI stained mouse C127 cell nucleus used for panels (**b**–**e**) (Supplementary Data S1). Data acquired on a GE OMX V3 Blaze instrument. Panels A1-A3 show the same plane with each of the three illumination angles. Insets show two-fold magnified and intensity-normalized view of the boxed region. Note the low contrast of the stripe pattern due to extensive out-of-focus blur contribution. (**b**) *Channel Intensity Profiles*, with total intensity variation (TIV) expressed as % within slices of a central 9-z-window in the three angles (marked light grey). In this example images from angle 3 show a markedly decreased intensity level (while there is little bleaching and intensity fluctuations) accounting for a total intensity variation of ~ 68%. (**c**) *Raw Fourier Projection* of the raw data in reciprocal space, with points of high-frequency information from first (inner) and second (outer spots) order stripes indicated by arrows. The presence of well-defined 1st and 2nd order spots in all three angles are a hallmark of optimal system calibration and generation of the structured illumination pattern. Arrowheads indicate less intense 2nd order spots in angle 3. (**d**) *Motion & Illumination Variation* assembly of phase-averaged and intensity-normalized images for each angle (left three panels, pseudo-coloured in cyan, magenta and yellow). The grey-white appearance of the CMY-merged output image (right panel) indicates motion stability and evenness of the illumination. (**e**) *Modulation Contrast* output with grey values indicating the modulation contrast-to-noise ratio (MCNR) values (left panel, greyscale). These values are then Otsu thresholded to select features and calculate a mean feature MCNR (central panel). The final representation uses a custom look-up-table to generate a heatmap of local MCNR values (right panel). Arrows indicate regions of saturated pixels with accordingly lower modulation contrast.
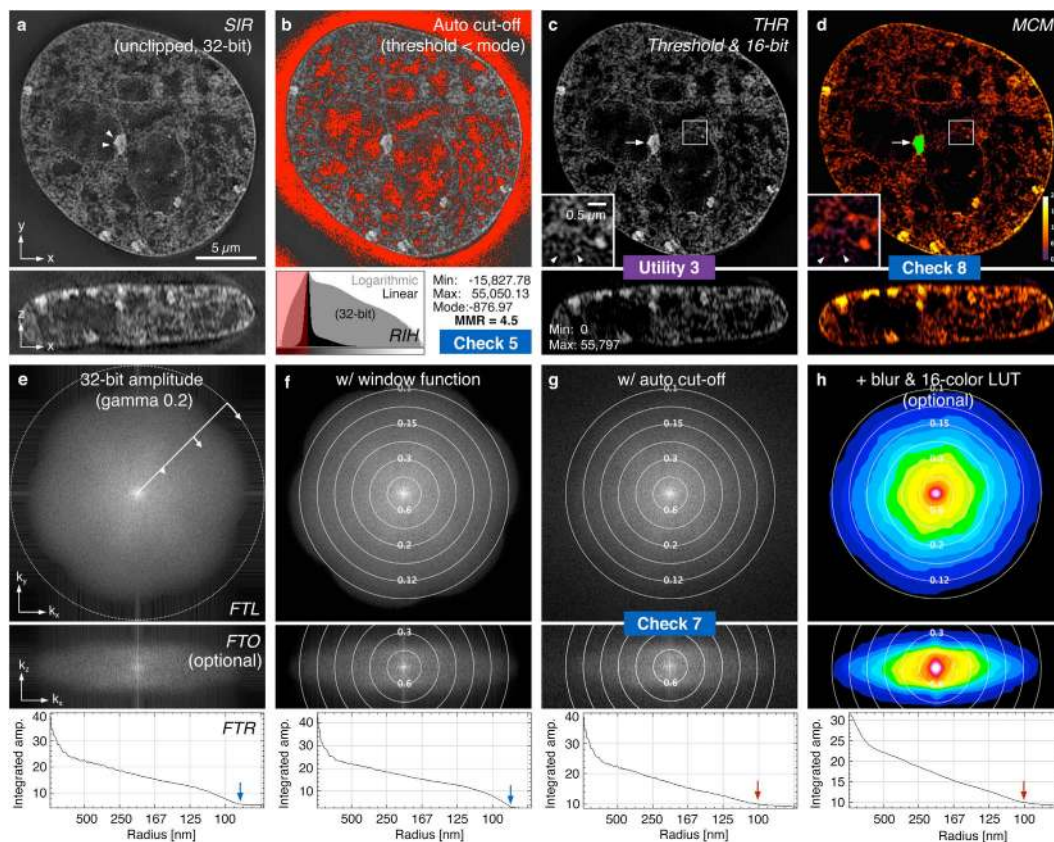
**Figure 3. SIMcheck output for reconstructed SIM data.** (**a**) Lateral and orthogonal cross section of reconstructed data used for panels (**b–h**), generated from raw data displayed in Fig. 2. (**b**) *Reconstructed Intensity Histogram* (bottom panel) showing the distribution of pixel intensities within the 32-bit data set on linear and logarithmic scales. Upper panel shows the areas below the mode intensity value that are discarded during thresholding. (**c**) The *Thresholding & 16-bit conversion* utility generates auto-thresholded composite TIFF stacks for further analysis and visualization (see also Supplementary Fig. S7). (**d**) *Modulation Contrast Map* combining the pixel intensity information of the reconstructed image with the colour information of respective MCN values (from Fig. 2e). Green colour indicates saturated pixels in the raw data that causes local reconstruction artifacts (arrow). Arrowheads in inset denote features in the nuclear interior of low modulation contrast (purple colour) in the corresponding raw data, compared to features with high underlying modulation contrast (orange-yellow) in the nuclear periphery. (**e–h**) Fourier spectra display variations of lateral FFT (FTL, top), orthogonal FFT (FTO, middle) and radial profile plot (FTR, bottom; orientation indicated in e, top panel). (**e**) 32-bit gamma 0.2 corrected amplitude Fourier spectrum of unclipped reconstructed data from (**a**). (**f**) Output with a window function applied to remove edge artifacts visible as horizontal and vertical stripes in (**e**). Overlaid concentric rings denote the respective spatial resolution (in μm). Note the distinct "flower" pattern with a prominent drop-off of the corresponding radial profile. The inflection point at ~90 nm (blue arrows) provides an approximation of the channel-specific frequency support. (**g**) Output of the mode-thresholded data shown in (**c**). The less pronounced frequency drop-off reflects the frequency mix of features and noise in the remaining (positive) intensity range after clipping the lower (negative) half of background (noise) intensities. The inflection point of the radial profile levelling with the amplitude background at ~100 nm (red arrows), provides an approximation of the effective resolution limit of features in the reconstructed data (see also Supplementary Fig. S8). (**h**) Output with optional additional colour-coding (right) applied in lateral and orthogonal Fourier spectra.

OMX) format suitable for analysis with *SIMcheck* (Supplementary Fig. 3). *Raw SI to Pseudo-Widefield* averages images from the raw structured illumination data and assembles an image equivalent to conventional widefield illumination, allowing for comparison of super-resolution and conventional images (Fig. 4b, Supplementary Fig. S7). This can highlight the resolution improvement gained from using SIM, and identify artifactual bright features in regions with very low intensity in the pseudo-widefield image. As most downstream image processing and analysis tools require 16-bit images, inconsistency can arise in conversion of 32-bit reconstructed data into 16-bit formats. The *Threshold and 16-bit Conversion* utility discards intensities below an adjustable threshold (by default the stack's modal intensity value), and

**Figure 4. SIMcheck output for SIM calibration data and utilities.** (**a**–**c**) 3D SIM data of a field of 0.1 μm diameter red fluorescent beads. (**a**) Representative central images of the raw data stack with the corresponding orthogonal views for each angle, and the *Raw Fourier Projection* output (bottom central panel). (**b**) Output from the *Raw SI to Pseudo-Widefield* utility, with orthogonal view and inset showing the dataset at conventional resolution. (**c**) Corresponding output from the *Threshold & 16-bit Conversion* utility demonstrating the increase in resolution and efficient rejection of out-of-focus blur. (**d**) *Illumination Pattern Focus* calibration tool applied to a field of red fluorescent beads imaged with two different system calibration settings showing orthogonal projections along the direction of the stripes for each angle. Top panel: single layer appearance with only weak, symmetric side lobes indicate good alignment of the axial illumination modulation with the focal plane. Bottom panel: zipper-like appearance indicates defocussing of the z-modulation for all three angles. (**e**,**f**) *Spherical Aberration Mismatch* check applied to a reconstructed dataset from a green fluorescent bead layer acquired under optimal (**e**) and suboptimal (**f**) imaging conditions, respectively. The intensity plot and the orthogonal cross section in **f** show a prominent dip in intensity underneath the bead layer (red arrow; white arrowheads), indicating a mismatch between sample/system conditions and the OTF used for the reconstruction. The corresponding z-minimum variation (ZMV) value relative to the average feature intensity (double arrows) is about three fold higher. (**g**) Output of the *Illumination Phase Step* utility of a dataset acquired from a green bead layer. The left panel shows a representative 2D FFT with the central area with the highest amplitude blocked. Yellow rings indicate auto-detected pixel positions of the highest intensity spots, normally associated with the first order stripes of the illumination pattern. The right panel displays a plot of the phase values in radians at these spots for all phase positions within a defined z-range (in this example ±1 z-sections around plane of best focus).

fills the 16-bit range of the converted image (Figs 3c and 4c, Supplementary Fig. S7). This tool facilitates higher standards in data handling and reporting for image analysis.

## Conclusion

Understanding how to verify instrument performance, tune parameters, and recognize artifacts are essential to obtaining optimal and reproducible super-resolution SIM data. The tools contained in *SIMcheck* enable general users and specialists to diagnose problems they encounter in acquiring and processing SIM data. In combination with careful system calibration and sample preparation protocols, as well as a comprehensive approach to experimental design, execution, and analysis, *SIMcheck* helps SIM systems perform to their full capability. This toolbox will facilitate establishing best practice in generating and

interpreting SIM images, making the technique much more accessible to the wider biology community, and ensuring super-resolution imaging fulfils its great potential.

## Methods

**Installation and quick start.**   The *SIMcheck* code is designed to run with the standard *ImageJ* (1.49 or newer) software package, requiring in addition a current version of *Bioformats Importer* plugin installed. Alternatively, it can be run with an up-to-date *Fiji* distribution of *ImageJ*[19] that includes the plugin by default. For installation the SIMcheck.jar file is copied into the Plugin folder of *ImageJ/Fiji* before restarting. Installing with *Fiji* offers the possibility for automatic updates by activating the *SIMcheck* update site in the *ImageJ Updater* accessible from the top down menu (*Help -> Update Fiji -> Manage update sites*). When importing raw data through *Bioformats Importer*, the "Stack Viewing" option must be set to "Hyperstack". The suite with four *Raw Data Checks* and four *Reconstructed Data Checks* can either be run in batch mode selected from the main *Run SIMcheck* dialog, or as stand-alone tests with extended options (Supplementary Fig. S1). In addition, two *System Calibration Tools* and four *Image Processing Utilities* are provided. The main dialog prompts the user to define the raw and/or reconstructed dataset to be analysed, the data format (GE OMX (default), Zeiss Elyra or Nikon N-SIM for conversion) and the camera bit-depth of the imaging system (to identify saturated pixels). It further enables cropping of both raw and reconstructed datasets to the same boundaries in x, y and z for specific analysis of defined sub-regions. The <help> button in the main dialogue links to an *Online Manual* that provides step-by-step guidelines how to use each tool and interpret its outcome. Note that the *Reconstructed Intensity Histogram (RIH)* and *Spherical Aberration Mismatch (SAM)* checks (see below) rely on reconstructed data still comprising the full histogram range. Clipping the low intensity range (the default setting in commercial reconstruction software) will also affect the output of the *Reconstructed Fourier Plots* (see below).

**Raw Data Checks.**   *Channel Intensity Profile (CIP).*   The check plots the absolute (slider position 1) and relative (slider position 2) average intensity for each plane (in the order: phase, z, angle, time) where each channel is assigned an arbitrary colour: 1st channel = red, 2nd = green, 3rd = blue, subsequent channels = black (Supplementary Fig. S3). Several intensity statistics are also calculated, including a summary statistic, total intensity variation (TIV) reporting the min-max range as a percentage of the maximum intensity for a 9-z-window about the central slice, over all phases and angles used in the reconstruction. A window size of ±4 z-sections was chosen, as the algorithm requires adjacent sections of the raw data stack to reconstruct a single 3D-SIM section and thus could contribute to potential artifacts. Three more specific statistics based on mean slice intensities help identify the type of intensity fluctuations present: (1) estimated intensity decay, which denotes the relative fluorescence decay per angle (averaged over all angles), as a measure of photobleaching; (2) maximum intensity difference between angles, which denotes the maximum difference between any two angles as a percentage of the maximum angle intensity; (3) relative intensity fluctuations ("flicker"), which denotes the average over all phases and angles of the min-max range over a 9-z-window about the central slice.

*Raw Fourier Projection (FPJ).*   This check applies a Gaussian windowing of 6% of the image width prior to carrying out a 2D Fourier transform (FFT) calling ImageJ's *FHT* routine, which returns a 32-bit logarithmically scaled amplitude squared [$\log(\text{amplitude}^2)$] Fourier spectrum that particularly amplifies the relevant high frequency range. Subsequently a maximum intensity projection over all phases and angles is generated from the resulting FFT stacks for each channel. The central circular region (diameter 1/8 of image width) is then filled with the minimum amplitude value before rescaling (min-max) to provide optimal contrast (Supplementary Fig. S4). The resulting Fourier projection highlights spots corresponding to the first and second order stripe frequencies in the illumination pattern for each angle. This check requires that the sample fills a significant proportion of the volume and that the signal-to-noise is adequate, in order to see second order spots. Sparsely fluorescent samples, such as isolated point-like objects would not show prominent spots even though the data quality may be sufficient. Also, FFT of 2D-SIM images acquired in TIRF mode would not show any spots, because the detection numerical aperture (NA) of the TIRF objective is significantly smaller than the excitation NA, preventing the detection of high frequency stripes in the excitation. Because of these specific requirements the check is by default not activated when running *SIMcheck* from the main dialog.

*Motion & Illumination Variation (MIV).*   The phases (default 5) from each angle at each z-plane are averaged and then each angle (assumes 3) is intensity-normalized before assigning a false colour cyan, magenta, or yellow (Supplementary Fig. S5). In this way features present in all angles will appear grey to white, while either movement of certain features or variations in illumination from the different angles, will exhibit an angle-specific colour. The colour scheme chosen here is intended to make the distinction between angles and channels clear. The reconstruction algorithm assumes that all features are sampled at each angle, and features that move significantly during the acquisition of a 3D frame or experience very different illumination intensity for different angles will result in artifacts. Of note, because of the linear polarization of excitation along the direction of stripes, some regional variations would also be

observed in case of samples with polarization-dependent fluorescence excitability, such as actin fibres or microtubules, without causing any artifacts.

*Modulation Contrast-to-Noise (MCN).*   To obtain a measure of the local stripe contrast, the following calculation is carried out for each voxel in the real 3D image: (1) A variance stabilizing Anscombe transform[20] is performed so that noise follows an approximately Gaussian, rather than Poissonian, distribution. (2) A z-window is selected as $2^*z + 1$ (z = number of z-planes above and below to be combine with each z-plane) and all raw phase images within this window are stacked (the default z-window of $\pm 1$ z-sections increases signal-to-noise to a similar extent to the "band filtering" performed during reconstruction). These phase series are Fourier-transformed using a hand-coded multithreaded 1D discrete Fourier transformation along the dimension of the different phases. The result of this 1D Fourier-transformation allows separating the different frequency components of the raw data (Supplementary Fig. S6). (3) The power of the frequency components corresponding to the illumination pattern modulation are divided by the standard deviation of the highest frequency component for the same z-plane (taken to be dominated by noise). The frequency components of first and second order in the Fourier transformed stack are located at plane numbers: $L_{FT}$ $^*$ $O/N_p + 1$, with $L_{FT}$ = length of the above Fourier transformed data stack (e.g. 5 phases $^*$ 3 z-sections = 15), $N_p$ = number of phase shifts during data acquisition, and $O$ = order number (1 or 2). The modulation-contrast-to-noise-ratio value is calculated as $MCNR = \sqrt{M_{O1}^2 + M_{O2}^2}/std\,(N)$. Average modulation contrast for each channel is estimated using *ImageJ*'s Otsu auto-thresholding routine with the stack histogram. Finally, a suggested Wiener filter parameter is given (for GE Healthcare's SoftWoRx SI reconstruction) based on the following empirical formula: Wiener filter constant, w = 0.17/MCNR².

**Reconstructed Data Checks.**   *Reconstructed Intensity Histogram (RIH).*   Linear- and logarithmic-scaled intensity histograms (black and grey, respectively) showing relative contribution of values below the modal intensity value for background regions, which are due to reconstructed noise and ringing artifacts at the edge of high-intensity features (Supplementary Fig. S7). Only intensities at the extremes of the histogram are considered: by default the lowest and highest 0.05% of intensities, subject to a minimum of 100 pixels. The min-to-max ratio (MMR) reported is calculated as: Max* – Mode/|Min* – Mode|; where Min* and Max* are the averages of the lowest and highest intensity pixel values, respectively. The number of pixels in each average is also shown in case artifacts such as zeros from truncation in processing or saturated pixels in data collection are significantly skewing the values. For meaningful results, the check requires untrimmed reconstructed data covering the full intensity range, such that in the reconstruction settings of commercial software the option "discard negatives" (GE), "baseline cut mode" (Zeiss) or equivalent must be deactivated.

*Spherical Aberration Mismatch (SAM).*   This check plots the minimum values and the mean feature intensity values (selected by Otsu auto-thresholding) in each slice. The summary statistics reports the z-minimum variation (ZMV) as the standard deviation of the slice minima, normalized by the average feature intensity (Fig. 4e,f). The ZMV metric is useful as a relative measure for artifacts caused by spherical aberration mismatch between the sample and the optical transfer function (OTF) when comparing datasets of similar characteristics, but acquired under different imaging conditions or reconstructed with different OTFs. This check requires untrimmed data, and it works best with flat, high-contrast samples (e.g. layers of beads) and is by default not activated when running *SIMcheck* from the main dialog.

*Reconstructed Fourier Plots (FTL, FTO, FTR).*   This check carries out a 2D fast Fourier transform (FFT) for each slice of the reconstructed data set to return a 32-bit amplitude Fourier spectrum with a gamma correction applied (gamma = 0.2) to enhance visibility in the higher frequency ranges. It outputs a stack of transformed xy-slices (Fourier Transform Lateral, FTL) displaying absolute amplitude levels with a pre-set scaling (between 2 and 40), overlaid with concentric rings that indicate the corresponding spatial resolution (in μm), and a radially integrated profile plot of the central z-slice in the FTL result (Fourier Transform Radial, FTR) (Fig. 3e–h). The data is by default pre-processed by subtracting the lower half of the background noise intensities, defined by the stack mode (i.e. the peak of the stack histogram), to reduce the frequency contribution of reconstructed noise in the resulting FFT and to allow comparability with datasets that have already been clipped accordingly by the reconstruction software. It is important to note that automatic clipping only provides meaningful results if the data contains a sufficient fraction of label-free background, so that only pixels within background regions are set to zero. If the field of view (or cropped region of interest) contains very little background, the modal value may provide an erroneously high cut-off, which can lead to artificial "sharpening" of structures, with the radial profile extending beyond the theoretical frequency support (no inflection point). In this case the cut-off limit should be set manually (for 32-bit data acquired and reconstructed with the correct camera/background offsets, this value is typically around the zero level).

The stand-alone plugin allows additional options and combinations thereof: (1) deactivate auto-cut-off, or apply a manual cut-off value (default = 0); (2) apply a window function (6% width) to remove horizontal and/or vertical stripe artifacts in the Fourier spectrum (e.g. if no cut-off is applied or if sample

features extend over the image boundaries); (3) return auto-scaled (min-max) gamma 0.2 corrected amplitude Fourier spectrum, or a log(amplitude$^2$) power spectrum with subsequent mode-max rescaling of each slice to provide a normalized FFT stack with further enhanced higher frequency range contrast over the default display option; (4) additional blurring and false-colouring with a 16-colour look-up-table (LUT) to highlight frequency dependent gradient characteristics of the amplitudes in the FFT plots; (5) display an axial FFT plot from the central re-sliced xz-section interpolated to generate isotropic voxels (Fourier Transform Orthogonal, FTO) (Supplementary Fig. S8). Note that re-slicing is carried out using *ImageJ*'s built-in command, and the radial profile plot is generated using a modified version of Paul Baggethun's plugin: http://rsb.info.nih.gov/ij/plugins/radial-profile.html. Overlaid rings can be removed or flattened down using the respective commands from the *ImageJ/Fiji* the top down menu (*Image -> Overlay -> Remove Overlay*, or *Flatten*).

*Modulation Contrast Map (MCM).*   The *Modulation Contrast Map* displays the reconstructed data with the colour information from the raw data MCN plugin multiplied with the intensity for each pixel, normalized to the maximum intensity in the image. The result is an RGB image where the mapped colour of reconstructed features (real or artificial) indicates the underlying modulation contrast in the corresponding raw data. Lastly, voxels that are saturated in one or more angles in the raw data (based on camera bit depth) are coloured green to highlight regions with missing stripe information that may cause local artifacts (Fig. 3d, Supplementary Fig. S9).

**System Calibration Tools.**   *Illumination Pattern Focus (IPF).*   This is a calibration check designed to work best with a dense single layer of sub-resolution size fluorescent beads that provide a high-contrast images of continuous stripes. Data are pre-processed to normalize intensity and correct slice-to-slice flicker using a simple ratio of mean slice intensities (Supplementary Fig. S10). The first phase for each angle is taken and rotated so that it is vertically aligned. The rotated sub-stacks are re-sliced orthogonally for an xz-view, and a maximum-intensity projection is performed along the direction of the stripes. The separate angles are displayed and stacked as a montage providing a visual representation of the axial illumination pattern where the pattern's alignment with the image plane in focus can be assessed.

*Illumination Phase Steps (IPS).*   This calibration check again requires a dense sample such as a bead lawn. Raw data slices are Fourier-transformed, the high intensity regions around the origin and along both horizontal and vertical axes, are masked, and first order spots are detected over a specified z-slice range using *ImageJ*'s built-in *Process > Find Maxima* command (Supplementary Fig. S10). The phase of the illumination pattern thus detected are plotted as a phase series (radians, unwrapped) for each step. Numerical statistics report on phase step accuracy (phase step standard deviation) and phase offset stability (phase offset standard deviation).

**Image Processing Utilities.**   *Format Converter (GE OMX).*   Converts Zeiss and Nikon format SIM data into the GE OMX 's "CPZAT" (channel, phase, z-slice, angle, time) dimension ordering, since all of the check plugins assume and require this dimension ordering to work correctly (Supplementary Fig. S3).

*Raw SI to Pseudo Widefield (PWF).*   Generates a pseudo-widefield image by (1) averaging all phases and angles for each slice in a raw SIM dataset and (2) rescaling in x-y by a factor of two using a bicubic interpolation to adapt the pixel size to the reconstructed data for direct comparison (Fig. 4b, Supplementary Fig. S7). Optionally, "simple ratio" intensity normalization may be applied to correct for intensity fluctuations and bleaching.

*Threshold and 16-bit Conversion (THR).*   Discards intensities below a threshold (by default automatic to the stack mode, or manually-defined per channel) and converts the remainder to 16-bit data, filling the 16-bit range. The dataset may be saved as composite tiff-stack for further processing and analysis (Fig. 4c, Supplementary Fig. S7).

*Stack FFT.*   Applies a 2D Fourier Transform to each slice in a stack. By default this uses an extension ImageJ's FHT class to produce log-scaled amplitude images for the complex FFT result, and implements Gaussian windowing of 6% of the image width prior to padding with zeros and transformation (Supplementary Fig. S4). Optionally, the windowing percentage can be varied and the scaling method changed to a gamma correction of choice.

For further information and guidance on applying *SIMcheck* to your data, see the *SIMcheck* user manual at http://www.micron.ox.ac.uk/microngroup/software/SIMcheck.html.

Source data from all commercial platforms is available for testing as Supplementary Data (https://www.dropbox.com/sh/4deho8b9cyjb8u7/AABWRZvfGu6M2B6hnmz_qLxxa?dl=0). Details on sample preparation and microscope system configuration are available upon request.

# References

1. Hell, S. W. Far-field optical nanoscopy. *Science* **316,** 1153–1158 (2007).
2. Huang, B., Babcock, H. & Zhuang, X. Breaking the Diffraction Barrier: Super-Resolution Imaging of Cells. *Cell* **143,** 1047–1058 (2010).
3. Schermelleh, L., Heintzmann, R. & Leonhardt, H. A guide to super-resolution fluorescence microscopy. *J Cell Biol* **190,** 165–175 (2010).
4. Zhang, J., Campbell, R. E., Ting, A. Y. & Tsien, R. Y. Creating new fluorescent probes for cell biology. *Nat Rev Mol Cell Biol* **3,** 906–918 (2002).
5. Heintzmann, R. & Cremer, C. Laterally modulated excitation microscopy: improvement of resolution by using a diffraction grating. in *Proc SPIE* (Bigio, I. J. *et al.*) 3568, 185–196 (SPIE, 1999).
6. Gustafsson, M. G. Surpassing the lateral resolution limit by a factor of two using structured illumination microscopy. *J Microsc* **198,** 82–87 (2000).
7. Gustafsson, M. G. L. *et al.* Three-dimensional resolution doubling in wide-field fluorescence microscopy by structured illumination. *Biophys J* **94,** 4957–4970 (2008).
8. Schermelleh, L. *et al.* Subdiffraction multicolor imaging of the nuclear periphery with 3D structured illumination microscopy. *Science* **320,** 1332–1336 (2008).
9. Weil, T. T. *et al.* Drosophila patterning is established by differential association of mRNAs with P bodies. *Nat Cell Biol* **14,** 1305–1313 (2012).
10. Lesterlin, C., Ball, G., Schermelleh, L. & Sherratt, D. J. RecA bundles mediate homology pairing between distant sisters during DNA break repair. *Nature* **506,** 249–253 (2014).
11. Burnette, D. T. *et al.* A contractile and counterbalancing adhesion system controls the 3D shape of crawling cells. *J Cell Biol* **205,** 83–96 (2014).
12. Smeets, D. *et al.* Three-dimensional super-resolution microscopy of the inactive X chromosome territory reveals a collapse of its active nuclear compartment harboring distinct Xist RNA foci. *Epigenetics Chromatin* **7,** 8 (2014).
13. Rego, E. H. & Shao, L. Practical structured illumination microscopy. *Methods Mol Biol* **1251,** 175–192 (2015).
14. Engel, U. Structured illumination superresolution imaging of the cytoskeleton. *Methods Cell Biol* **123,** 315–333 (2014).
15. Turnbull, L. *et al.* Super-resolution imaging of the cytokinetic Z ring in live bacteria using fast 3D-structured illumination microscopy (f3D-SIM). *J Vis Exp* 51469 (2014). doi: 10.3791/51469.
16. Editorial. Seeing in super-resolution. *Nat Meth* **11,** 1183 (2014).
17. Schneider, C. A., Rasband, W. S. & Eliceiri, K. W. NIH Image to ImageJ: 25 years of image analysis. *Nat Meth* 96, 71–675 (2012).
18. Demmerle, J., Wegel, E., Schermelleh, L. & Dobbie, I. M. Assessing resolution in super-resolution imaging. *Methods* doi: 10.1016/j.ymeth.2015.07.001 (2015).
19. Schindelin, J. *et al.* Fiji: an open-source platform for biological-image analysis. *Nat Meth* **9,** 676–682 (2012).
20. Anscombe, F. J. The transformation of Poisson, binomial and negative-binomial data. *Biometrika* **35,** 246–254 (1948).

## Acknowledgements

## Author Contributions

G.B. and L.S. conceived the code. G.B. wrote it, with conceptual contribution from R.K. and I.M.D. assisted in its implementation. L.S., I.M.D. and J.D. tested performance and provided test data. L.S. and J.D. created the figures. G.B., J.D., I.D., I.M.D. and L.S. wrote the paper.

## Additional Information

**Supplementary information** accompanies this paper at http://www.nature.com/srep

**Competing financial interests:** The authors declare no competing financial interests.

**How to cite this article**: Ball, G. *et al.* SIMcheck: a Toolbox for Successful Super-resolution Structured Illumination Microscopy. *Sci. Rep.* **5**, 15915; doi: 10.1038/srep15915 (2015).

**Supplementary Information**

**SIMcheck: a Toolbox for Successful Super-resolution Structured Illumination Microscopy**

Graeme Ball[1,3], Justin Demmerle[1], Rainer Kaufmann[1,2], Ilan Davis[1], Ian M. Dobbie[1] & Lothar Schermelleh[1]

[1]Department of Biochemistry, University of Oxford, Oxford, UK.

[2]Division of Structural Biology, Wellcome Trust Centre for Human Genetics University of Oxford, Oxford, UK.

[3]Current Address: Dundee Imaging Facility, School of Life Sciences, University of Dundee, Dundee, UK.

Correspondence should be addressed to L.S. (lothar.schermelleh@bioch.ox.ac.uk).
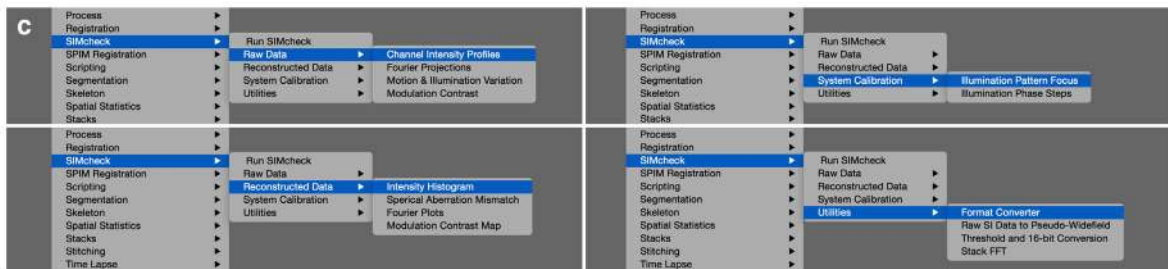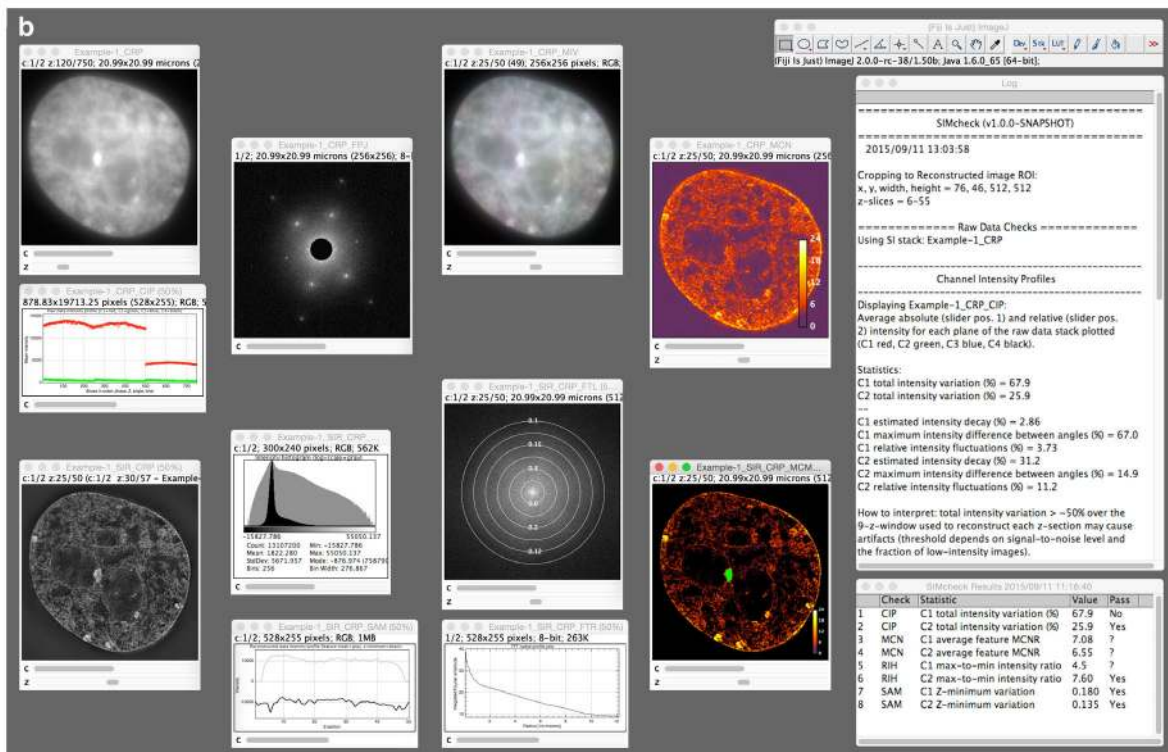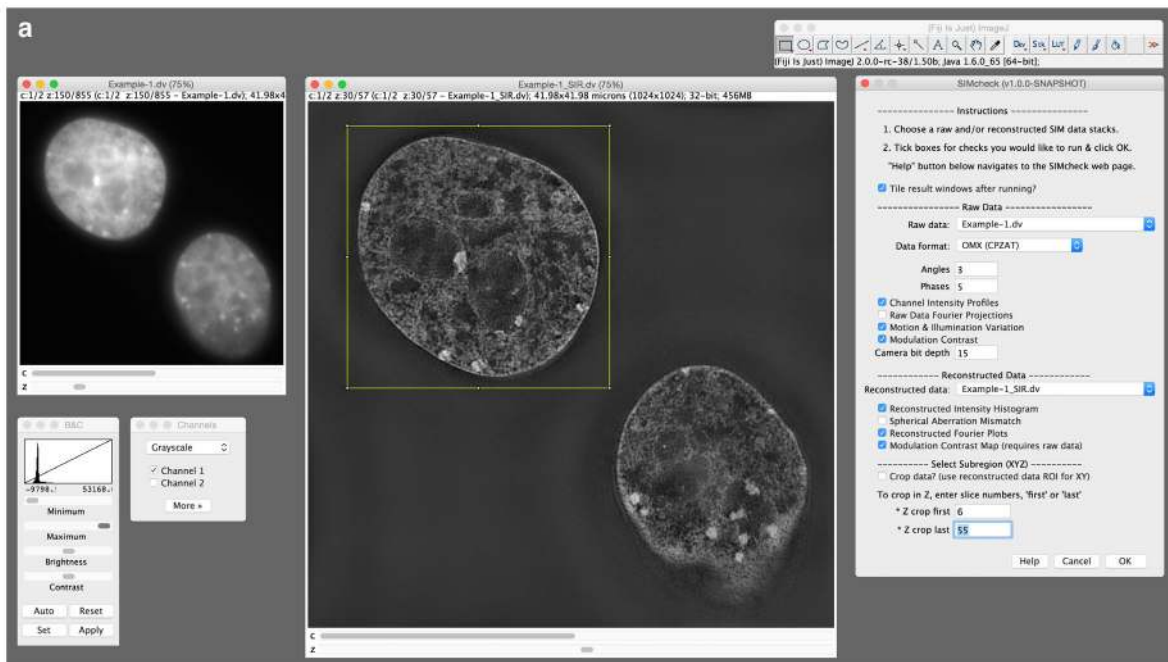
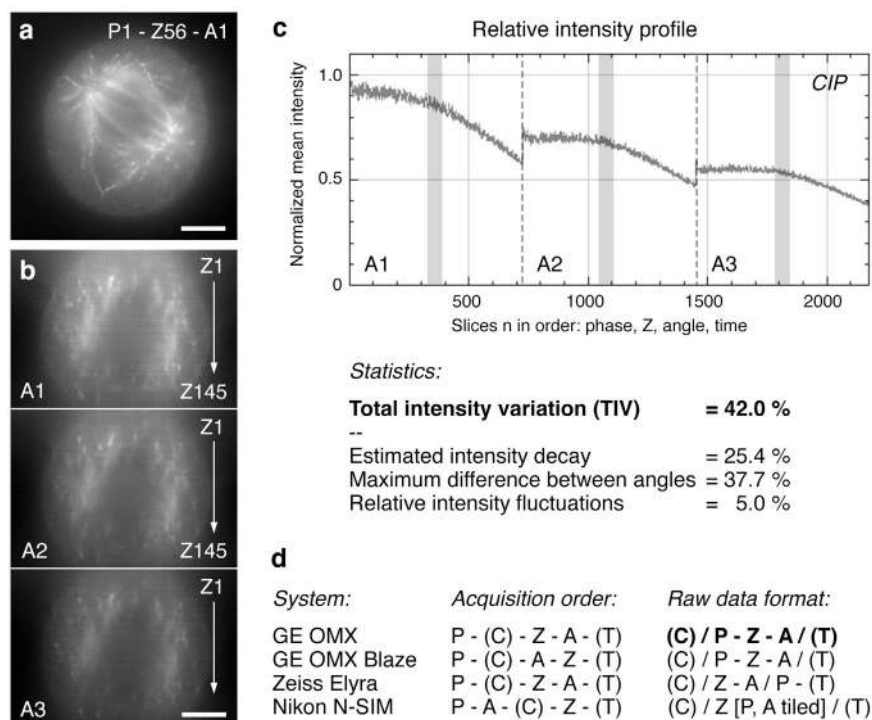**Supplementary Figure S1** | *SIMcheck* screenshots. (**a**) Screenshot of the *SIMcheck* main dialog after being opened in *Fiji/ImageJ* (top right, default settings), with raw data of DAPI stained mouse C127 cell nuclei (left, **Supplementary Data 1a**) and the corresponding, unmodified, reconstructed data (centre, **Supplementary Data 1b**). The upper cell is highlighted for cropping (512x512 pixel ROI using *Edit > Selection > Specify…*), limiting *SIMcheck* analysis to the selected region. Useful *B&C* and *Channels* tools (bottom left) are opened automatically when running *SIMcheck* from the main dialog box. (**b**) Screenshot of *SIMcheck* output with all raw and reconstructed data checks for channel 1 (DAPI; channel 2 not shown). In addition, a *Log* window providing a short description, extended results and interpretation for each check (right centre), and a *SIMcheck Results* window summarizing the most important metrics (right bottom). (**c**) Four screenshots illustrating the menu structure for all stand-alone plugins.

## Supplementary Table S2 | Notes and interpretation guidelines

| | | Function Title | Notes / About | How to interpret |
|---|---|---|---|---|
| **Raw data check** | 1 | Channel Intensity Profiles | Average absolute (slider pos. 1) and relative (slider pos. 2) intensity for each plane of the raw data stack plotted (C1 red, C2 green, C3 blue, C4 black). | Total intensity variation > ~50% over the 9-z-window used to reconstruct each z-section may cause artifacts (threshold depends on signal-to-noise level and the fraction of low-intensity images). |
| | 2 | Fourier Projection | Maximum intensity projection of log(amp$^2$) 2D FFT stack, with central area masked, and rescaled (min-max) to improve contrast of the relevant frequency range. | Look for clean 1st & 2nd order spots, similar across angles. Note that spot intensity depends on image content. |
| | 3 | Motion and Illumination Variation | Each angle phase-averaged, normalized, and false-colored (A1 cyan, A2 magenta, A3 yellow). | Non-white areas indicate differences between angles due to drift, floating particles or illumination variations. |
| | 4 | Modulation Contrast | Modulation contrast-to-noise ratio (MCNR) image. Average feature MCNR selected by auto-thresholding (Otsu).<br><br>Estimated Wiener filter parameter is valid for OMX data reconstruction (SoftWoRx) only. | Colour LUT indicates MCNR value:<br>• purple is inadequate (<4)<br>• red is low to moderate (4-8)<br>• orange is good (8-14)<br>• yellow-white is very good to excellent (>14) |
| **Reconstructed data check** | 1 | Intensity Histogram | Intensity counts in black (linear) & grey (log-scale).<br><br>MMR is calculated as the ratio of the averaged 0.001% highest (Max\*) and lowest (Min\*) intensity pixels in a 32-bit stack, centred at the stack mode (assumed to be the centre of the noise distribution), that is:<br>Max\* - Mode / \|Min\* - Mode\| | Max-to-min intensity ratio ranges: MMR <3 is inadequate, 3-6 is low, 6-12 is good, >12 excellent. For valid results, the data set must contain sufficient background areas (so that the mode reflects background) and should be constrained to z-slices containing features.<br><br>N.B. MMR statistic is only valid for unclipped data (reconstruction option 'discard negatives' or 'baseline cut mode' deactivated). |
| | 2 | Spherical Aberration Mismatch | Z-section minimum (black) and mean feature intensity (grey).<br><br>Z-minimum variation (ZMV) is calculated as the standard deviation of z-section minimum intensity normalized to the average feature intensity. | High ZMV indicates spherical aberration mismatch between the sample and the optical transfer function used for the reconstruction.<br>Typically this is seen as a dip in the minimum intensity plot at the sample boundary. Note that the absolute value depends on image content.<br>N.B. The ZMV statistic is only valid for unclipped data (reconstruction option 'discard negatives' or 'baseline cut mode' deactivated). |
| | 3 | Fourier Plots | Fourier Transform Lateral (XY; resolution rings in microns)<br>[Optional: Fourier Transform Radial profile (lateral, central Z)].<br><br>By default the reconstructed data are<br>(1) cropped to the mode intensity value and<br>(2) Fourier transformed and scaled by a gamma function (gamma=0.2). | Fourier plots highlight potential artifacts and indicate effective resolution:<br>• Spots in Fourier spectra indicate periodic patterns.<br>• A flattened Fourier spectrum (a plateau in the radial profile) indicates the lack of real high frequency signal and therefore poor resolution.<br>• Asymmetric Fourier spectra indicate angle-specific decreases in resolution due to any of the following: angle-to-angle intensity variations; angle-specific illumination pattern ('k0') fit error; or angle-specific z-modulation issues. |
| | 4 | Modulation Contrast Map | MCN: Reconstructed data color-coded according to the underlying Modulation Contrast-to-Noise Ratio (MCNR) in the raw data. | The MCNR map indicates local variations in reconstruction quality, e.g. variations in out-of-focus blur contributions due to feature density, or uneven patterning of the structured illumination.<br><br>MCNR values: 0-4 purple (inadequate), to 8 red (acceptable), to 12 orange (good), to 18 yellow (very good), to 24 white (excellent).<br><br>Saturated pixels detected in the raw data according to selected bit-depth are false-colored green. |
| **Calibration** | 1 | Illumination Pattern Focus | Projected side view along the illumination stripes (phase 1 only) for each angle to illustrate alignment of the illumination pattern's z-modulation with the focal plane. Slice intensities are normalized to correct for intensity variations. | 100 nm bead layer in the focal plane should display distinct intensity modulation (side view of first order stripes. Intensity dips above and below the intensity peaks should be balanced. A "zipper-like" appearance (i.e. two staggered layers of modulated intensities) indicates defocussing of the z-modulation against the focal plane. All angles should have the same characteristics. |

**c** Relative intensity profile

CIP

Normalized mean intensity
1.0
0.5
0

A1    A2    A3

500   1000   1500   2000

Slices n in order: phase, Z, angle, time

*Statistics:*

| | |
|---|---|
| **Total intensity variation (TIV)** | **= 42.0 %** |
| -- | |
| Estimated intensity decay | = 25.4 % |
| Maximum difference between angles | = 37.7 % |
| Relative intensity fluctuations | = 5.0 % |

**d**

| System: | Acquisition order: | Raw data format: |
|---|---|---|
| GE OMX | P - (C) - Z - A - (T) | **(C)** / P - Z - A / **(T)** |
| GE OMX Blaze | P - (C) - A - Z - (T) | (C) / P - Z - A / (T) |
| Zeiss Elyra | P - (C) - Z - A - (T) | (C) / Z - A / P - (T) |
| Nikon N-SIM | P - A - (C) - Z - (T) | (C) / Z [P, A tiled] / (T) |

(panel a label: P1 - Z56 - A1; panel b labels: Z1, A1, Z145, Z1, A2, Z145, Z1, A3)

**Supplementary Figure S3** | Generation of *Channel Intensity Profiles (CIP)*. (**a**) Raw data image stack of a HeLa cell immunostained for microtubules (detected with Alexa Fluor 488 conjugated secondary antibodies) acquired on an OMX V2 instrument (**Supplementary Data 2a**). From a central z-section (Z56), the image for phase step 1 (P1) of angle 1 (A1) is shown. (**b**) Orthogonal view of raw data stack with acquisition angles A1 - A3 and z-slices shown with the first slice (Z1) at the top, and the last slice (Z145) at the bottom for each angle (only P1 shown). Scale bar: 5 μm. (**c**) *SIMcheck* output with the relative mean intensity of each frame plotted on the y-axis, and the order of the slices, separated by angle, on the x-axis. Five phase steps (P1-5) are acquired per z-slice and angle, resulting in 145 x 5 = 725 images per angle in the dataset. The employed OMX V2 system uses a mechanical phase grating for the pattern generation and acquires image stacks for different rotation angles sequentially. Accordingly, fluorescence intensity decreases through the z-stack and with each consecutive angle due to photobleaching. Below is the corresponding *SIMcheck* log output, providing the total intensity variation (TIV) within a window of 9 central z-sections contributing to reconstruct one super-resolution z-section (marked light grey). In addition statistics on the average decay rate per angle, maximum intensity difference between angles and relative intensity fluctuations are provided to diagnose selective contributions to the TIV. (**d**) Table comparing the acquisition order and raw data format of the three commercially available SIM platforms. GE's OMX platform comes with either a rotary diffraction grating (V2/V3) where angle rotation is the last step, or a rapid angle-switching device (V3/V4 Blaze), which has a different acquisition order. It should be noted that acquisition on these instruments may be switched by the user between "all channel then Z" or "all Z then channel". While the raw data format varies between manufacturers, *SIMcheck* is written to accommodate by default the GE data format, and therefore datasets from other manufacturers need to be converted either from the main dialog or separately with the *Format Conversion* tool prior to analysis with any of the stand-alone checks and utilities.
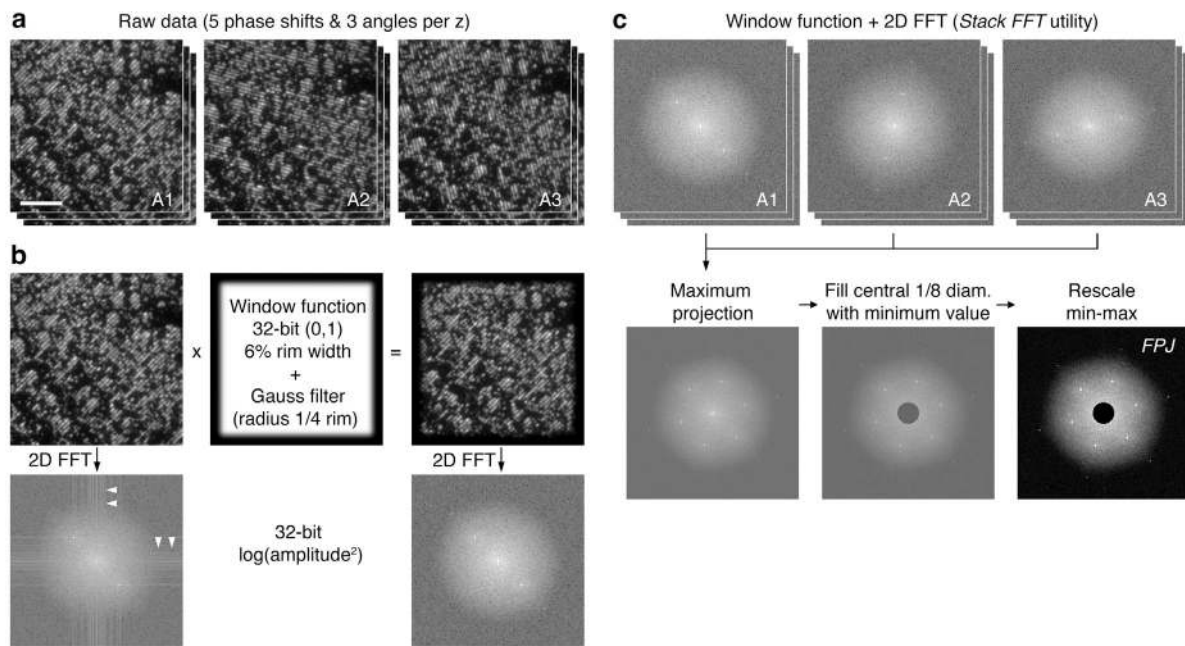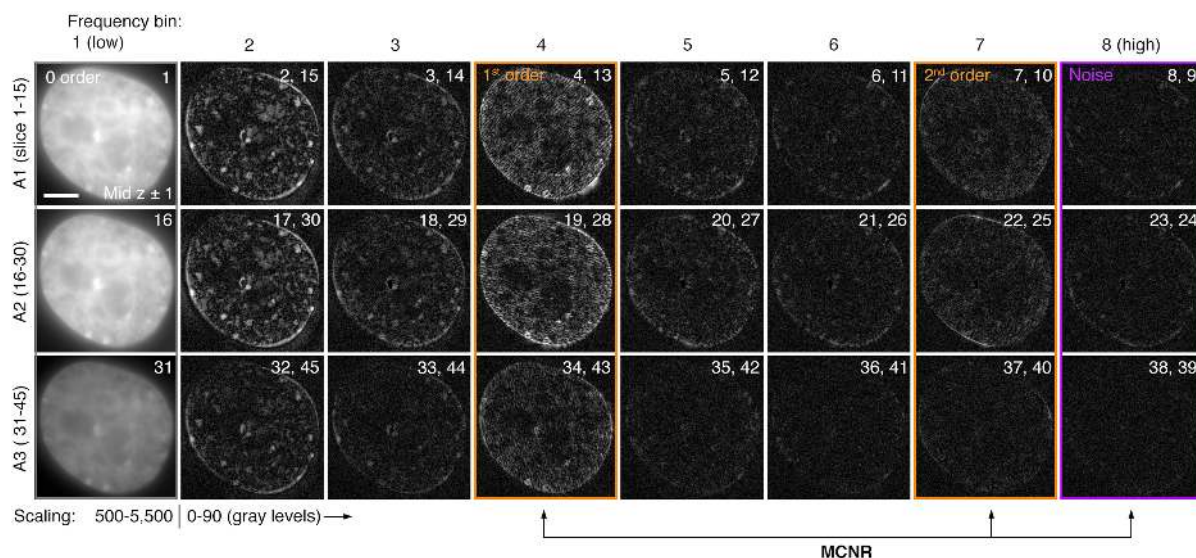
**Supplementary Figure S4** | Generation of raw data *Fourier Projection (FPJ)*. (**a**) Raw data from a field of green 110 nm diameter fluorescent beads (FluoSphere 505/515, Life Technologies), demonstrating how each illumination angle is considered as a separate z-stack for the construction of the *Raw Fourier Projection (FPJ)* check. Data acquired on a GE OMX V3 Blaze instrument (**Supplementary Data 3a**). Scale bar: 5 µm. (**b, c**) Illustration of intermediate processing steps to generate the final *FPJ* output. (**b**) A 2D fast Fourier transform (FFT) is applied to generate a 32-bit amplitude$^2$ Fourier power spectrum that is logarithmically scaled to enhance detection of high frequencies. Middle panel shows a diagrammatic representation of the window function that is multiplied to each raw data image before applying the FFT. This removes "edge artifacts" that otherwise appear as stripes along the axes of the Fourier spectrum of unprocessed data (bottom left, arrowheads). (**c**) An intermediate FFT stack is assembled (*Stack FFT* utility) and a maximum intensity projection generated over all three angles combined. For the final output the central region is masked before rescaling to enhance the contrast of the relevant higher frequency range. The processing steps enable at a glance to assess the presence and quality of first (inner) and less intense second order (outer) spots, corresponding to first and second order stripes in the structured illumination pattern.
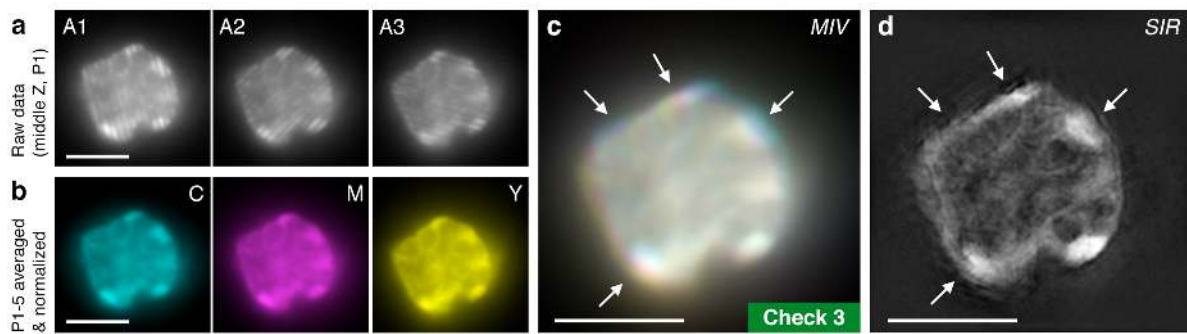
**Supplementary Figure S5** | *Motion & Illumination Variation* check. (**a**) Raw data from a DAPI stained nucleus of a fixed, non-adherent mouse hematopoietic stem cell, showing one phase of each angle of a representative mid section (A1-A3 respectively). Data acquired on a GE OMX V2 instrument. (**b**) Data from **a** with average projection of all 5 phases, intensity normalization and color-coding (cyan, magenta, yellow) by angle. (**c**) Merge of the three panels in **b** result in a largely white "colocalization" image, but motion artifacts are illustrated around the edges of the nucleus, indicated by one colour predominating (arrows). (**d**) Reconstructed data from **a**, showing artifacts resulting from motion (arrows). Scale bar: 2 μm.

**Supplementary Figure S6** | *Modulation contrast-to-noise* (MCN) calculation. Intermediate processing steps of the raw data corresponding to **Fig. 2e** is shown after 1D discrete Fourier transformation along the phase dimension to separate frequency components in the central ±1 z-planes (see **Methods**). Rows are arranged by angle (1-3), while slices indicate origin of each subsequent panel in each row. For the final MCN output all three angles are combined. Columns, containing equivalent data from each angle, indicate steps in processing, and progress from left to right in order of frequency information, from low to high. Numbers in the panels indicate their absolute position in the stack during processing, and ascend or descend relative to the position of the first (leftmost) column. The first, fourth, and seventh columns represent information generated by zero, first, and second-order stripes resulting from the interference of the structured illumination pattern and the sample, while the intermediate panels show intermediate steps taking during processing in *SIMcheck*. The rightmost column shows the noise contribution to the preceding images in each row. The MCNR value is calculated on a per-pixel basis as the ratio between and the first- and second order contribution shown in the fourth and seventh column (average of each pixel) and the noise contribution (1x StdDev over the whole image) shown in the rightmost column. Scale bar: 5 μm.
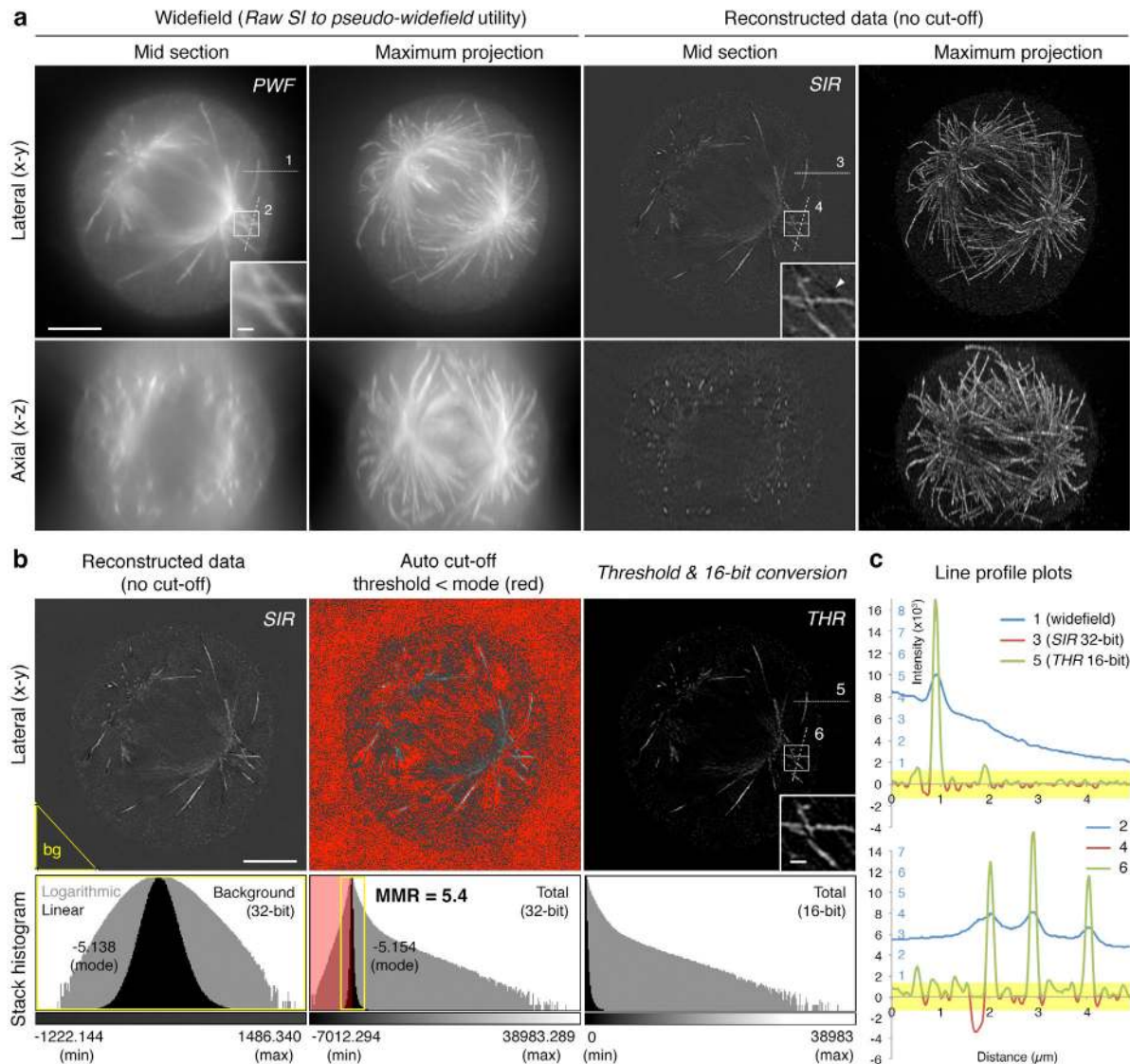
**Supplementary Figure S7** | Image processing tools and intensity histogram analysis. (**a**) Dataset recorded of a mitotic HeLa cell immunostained for microtubules acquired on a GE OMX V2 instrument (see also **Supplementary Fig. S3**). Left panels: Conventional widefield resolution image stack was generated with the *Raw SI to Pseudo Widefield* utility. Right panels: Auto-scaled reconstructed data without further post-processing (**Supplementary Data 2b**). Grey colour in the background area of the mid section is due to the presence of darker regions above and below brighter features (inset, arrowheads). Maximum intensity projecting of the entire stack levels the background intensities due to the stochastic nature of the reconstruction noise. Scale bar: 5 μm (inset 0.5 μm). (**b**) Left panel: Stack histogram of the background area (bg, yellow triangle in lateral section) indicates a symmetric (Poisson) distribution of the noise around the modal value between ~ ±1,300 grey levels. Central panel: Pixel intensity values below the mode are coloured in red. The yellow box in the stack histogram indicates the range of the reconstruction noise. Values below this band originate from intensity dips surrounding brighter features. These become more prominent under suboptimal imaging conditions, particular with spherical aberration mismatch. The min-to-max-ratio (MMR) provides a metric for the degree of reconstruction artifacts in the dataset. Right panel: Same data set after applying the *Threshold & 16-bit Conversion* utility.

All values below the stack mode (default option, valid if the data contains a sufficient background area) are truncated and the dataset converted to a 16-bit composite TIFF without contrast stretching. (**c**) Intensity profile plots along the lines indicated in panels **a** and **b** demonstrating the x-y resolution doubling and massive contrast enhancement in the reconstructed data compared to the conventional widefield image. Reconstruction noise (yellow band) fluctuates around the mode threshold (~0; this value may vary between datasets depending on camera offset setting and sample conditions). After the noise cut-off, about half of pixel values within the background regions are still above this threshold, thus avoiding the uncontrolled eradication of reconstruction artifacts. Scale bar: 5 µm (inset 0.5 µm).
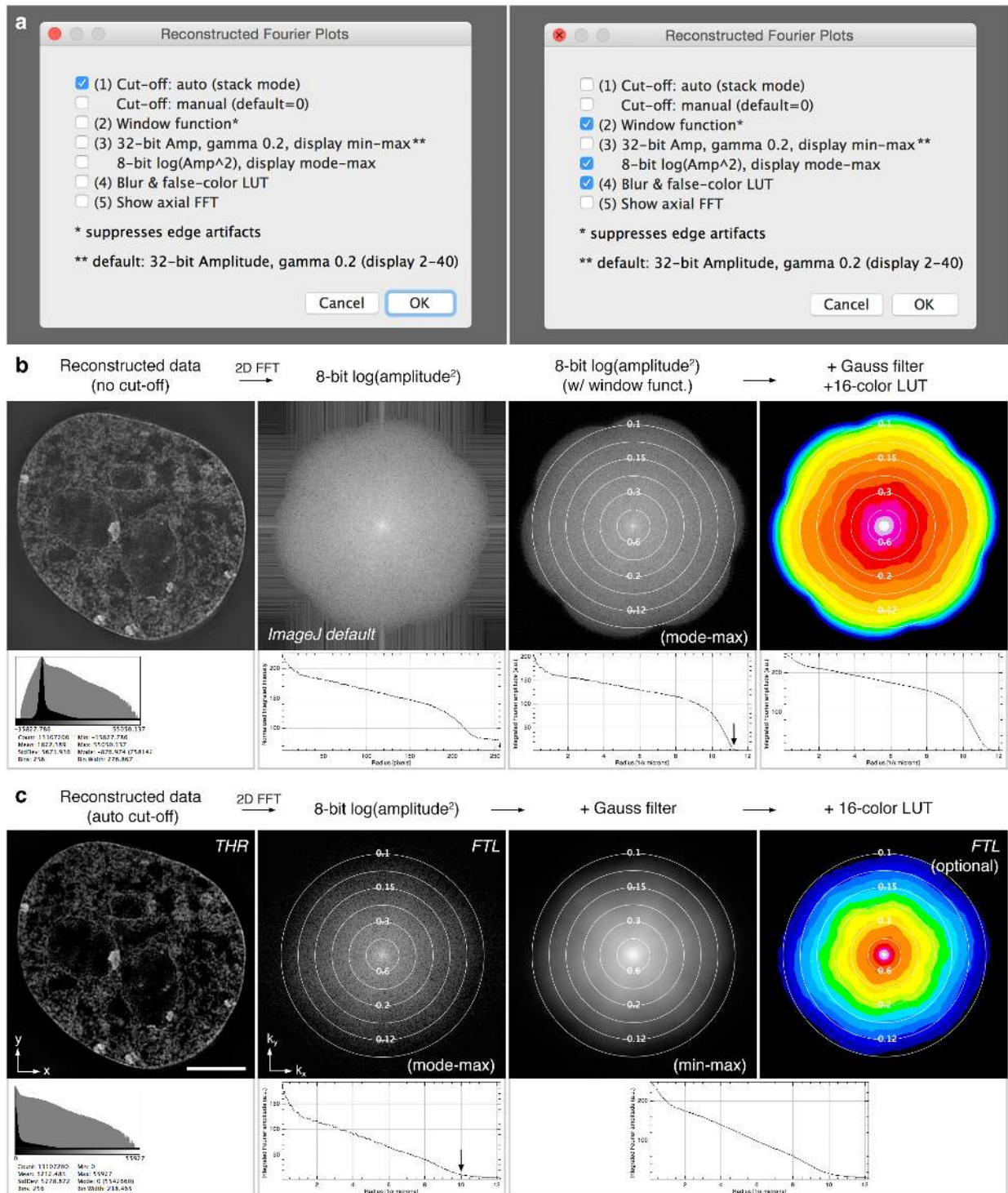
**Supplementary Figure S8** | Display options for *Reconstructed Fourier Plot*. (**a**) Screenshot of the option menu specifically available to the stand-alone plugin, with default settings (left) and optional settings activated (right). (**b**) Display options without input data cut-off. Left panel: lateral mid section of the same reconstructed dataset as shown in **Fig. 3** with corresponding stack histogram and statistics displayed below. Second panel: 8-bit converted log-scaled (amplitude$^2$) power spectrum as generated by *ImageJ*'s default FFT function, with corresponding radial profile plot below. Third panel: *SIMcheck* result with active window function and display set to *8-bit log(amplitude$^2$)*, to remove edge artifacts and

amplify the high frequency range (compared to the default gamma correction; see **Fig. 3**). Overlaid concentric rings denote the respective spatial resolution (in µm). Arrow in the radial profile indicates the system- and wavelength-dependent limit of the frequency support (1/~11 µm = approx. 90 nm). Note that the resolution on the x-axis is provided as reciprocal distance. Right panel: display option with additional blurring and false-colouring to visually support the gradient characteristics of the frequency distribution by concentric coloured rings. (**c**) Left panel: Mid section of the same dataset after applying auto cut-off (threshold < stack mode). Second panel: log(amplitude$^2$) power spectrum and corresponding radial profile show less prominent drop-off due to removal of reconstructed noise in the negative range of the 32-bit reconstructed data. Arrow points to the inflection point between amplitude drop-off and FFT background that provides an approximation of the effective resolution limit in the data (1/~10 µm = approx. 100 nm). Intermediate blurring step before (third panel) and after false-colouring (right panel).
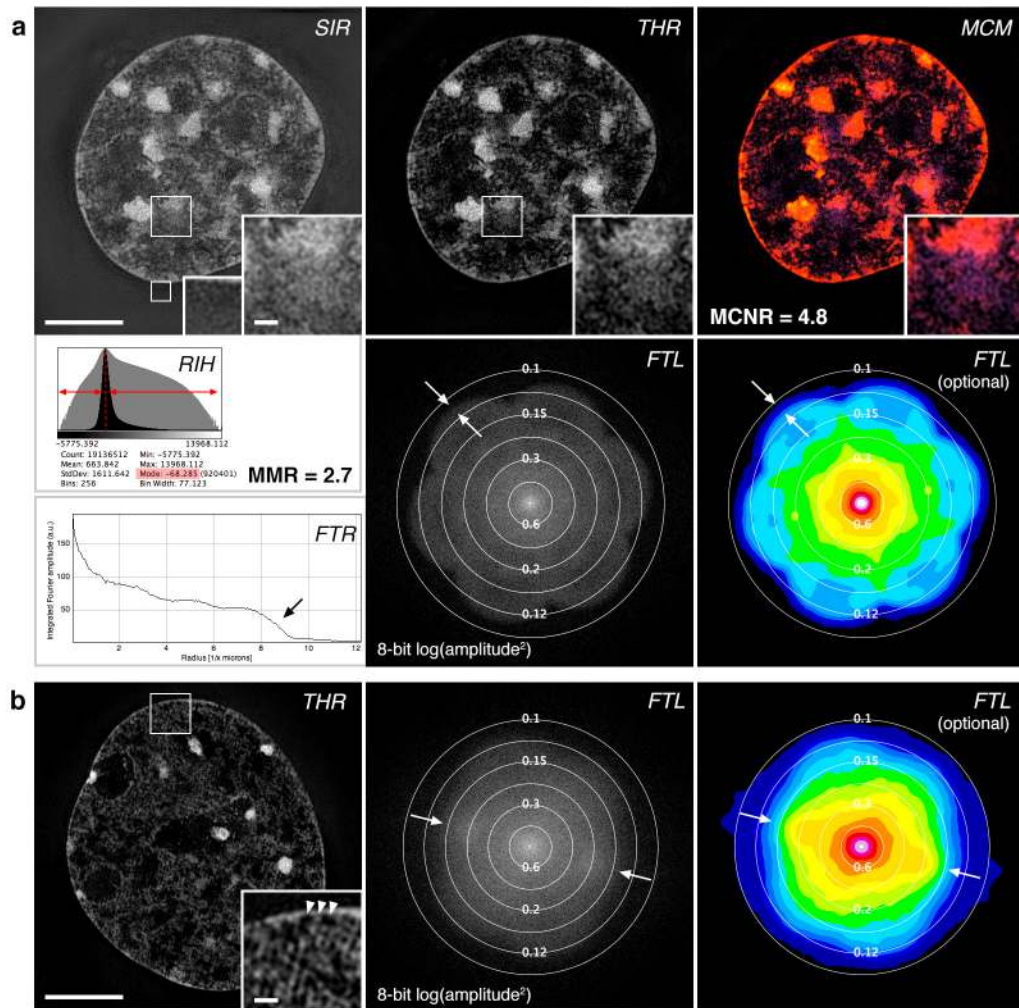
**Supplementary Figure S9** | Identification of signal-to-noise and angle-specific artifacts. Reconstructed data from DAPI stained mouse C127 cell nuclei. (**a**) Mid section of unprocessed reconstructed data shows prominent small-scaled "curly" features (large inset, top left panel). Similar albeit weaker features are apparent from reconstructed noise in background regions (small inset, top left panel). These structures are still visible after clipping to the mode (inset, top middle panel). Mapping of the local MCNR values indicate very low underlying modulation contrast in the corresponding raw data (inset, top right panel) and a low average feature MCNR of 4.8 (threshold for acceptable reconstruction ~8). The corresponding intensity histogram provides a min-to-max ratio (MMR) of 2.7 (threshold of ~3 for acceptable reconstruction). The corresponding log-scaled Fourier plots (FTL, FTR) of the thresholded data show a sharp drop-off at the edge of the frequency support (arrows, lower panels). (**b**) Mid section of thresholded reconstructed data showing a stripy appearance in one angle direction (arrowheads in inset, left panel). The lateral Fourier plots show a skewing in the corresponding perpendicular orientation (middle and right panel, arrows), indicating reduced resolution in one angle, in this case caused by a false k0 angle reconstruction parameter.
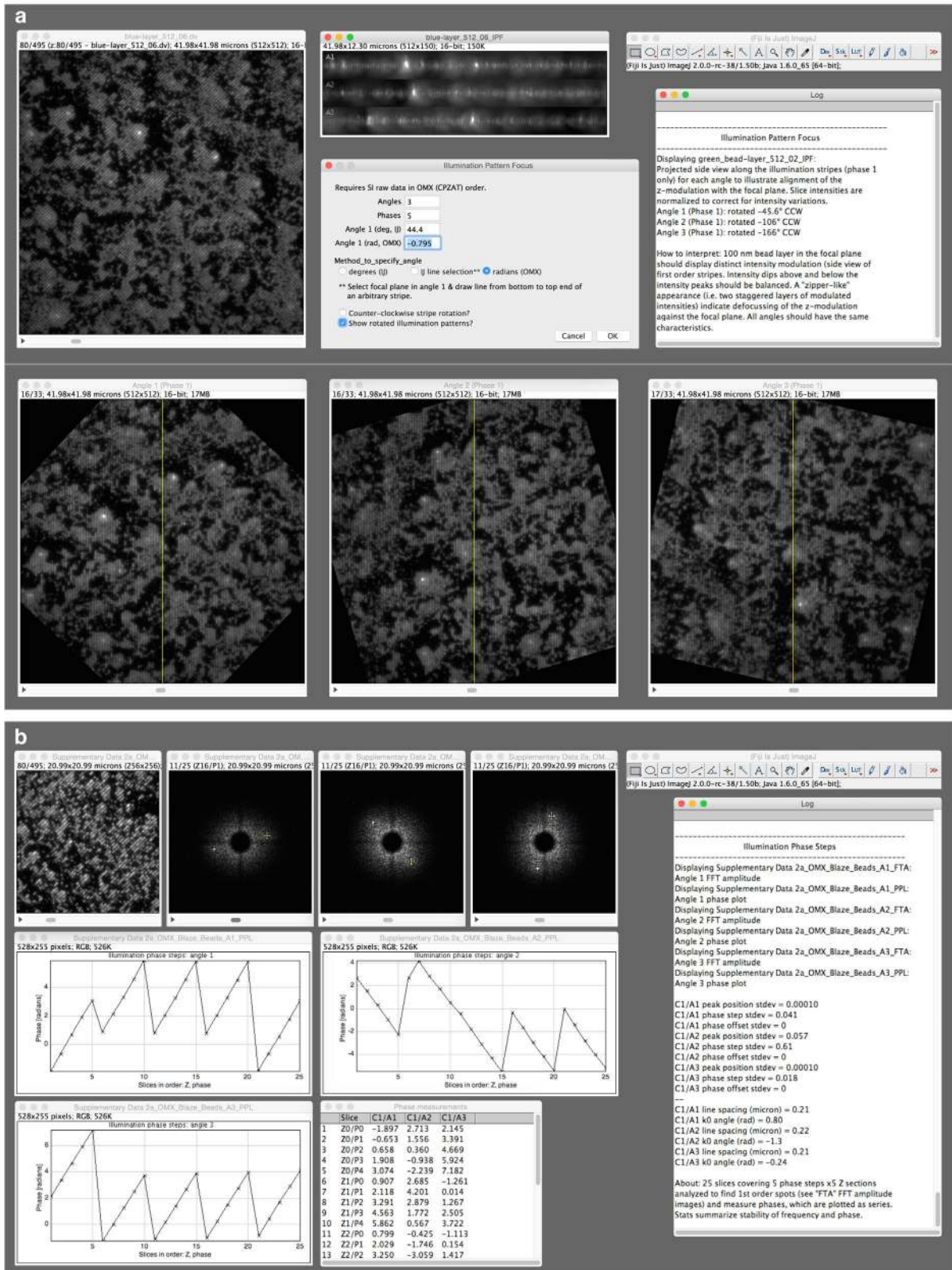
**Supplementary Figure S10** | *Illumination Pattern Focus* and *Illumination Phase Steps* calibration tools. (**a**) Screenshot of the *Illumination Pattern Focus* tool applied on a raw SI dataset of a field of blue 110 nm fluorescent beads (FluoSpheres 350/440; Life Technologies) acquired with a GE OMX V3 Blaze system. Top left panel: Raw data

window. Top central upper panel: Result window with maximum intensity projected orthogonal views of the 1$^{st}$ order stripe pattern along the bead layer. Top central lower panel: Main dialog providing different options to define the first pattern rotation angle. Top right panel: Log output, including degree of rotation for each angle of the raw data, as well as suggestions for interpretation. Lower panel: Optional display of the separated angles (phase 1 only, images of phase steps 2-5 discarded) after rotation to the same vertical orientation. (**b**) Screenshot taken after running the *Illumination Phase Step* calibration on a dataset acquired from a green 100 nm bead layer with a GE OMX V3 Blaze instrument. Top left panel: Raw data window. Top central panels: angle specific (angles 1-3, respectively) FFT stacks for all phase positions within a defined z-range (in this example ±2 z-sections around plane of best focus). Central area with the highest amplitude is blocked. Yellow crosses indicate the pixel position of the highest intensity spots (identified by the *ImageJ*'s *Find Maxima* process), typically associated with the first order stripes of the illumination pattern. The windows below display plots of the phase values in radians at these spots for each angle (angles 1-3, respectively), as well as the measured values in a results table for export into a spreadsheet program for further analysis. The log window on the right provides information on the angle and stripe width.

**Supplementary Table S11** | *SIMcheck* beta testers

| Name | Affiliation | Location |
|------|-------------|----------|
| Julio Mateos Langerak | CNRS Montpellier | FR |
| Theresa Swayne | Columbia University | US |
| Andreas Bruckbauer | Crick Institute London | UK |
| Edmundo Sanchez Guajardo | CSF Vienna Biocenter | AT |
| Lijuan Zhang | CSF Vienna Biocenter | AT |
| Kareem Elsayad | CSF Vienna Biocenter | AT |
| Andre Lampe | FMP Berlin | DE |
| Jan Schmoranzer | FMP Berlin | DE |
| Martin Lehmann | FMP Berlin | DE |
| Milos Sramek | GMI Vienna | AT |
| Matthew Pearson | IGMM University of Edinburgh | UK |
| Ann Wheeler | IGMM University of Edinburgh | UK |
| Jaron Liu | IMB Singapore | SG |
| Karin Aumayr | IMP Vienna | AT |
| Pawel Pasierbek | IMP Vienna | AT |
| Debora Keller | Imperial Collage London | UK |
| Tristan Piolot | Institut Curie Paris | FR |
| Orestis Faklaris | Institut Jacques Monod Paris | FR |
| Audrey Salles | Institut Pasteur Paris | FR |
| Eva Wegel | John Innes Centre Norwich | UK |
| Grant Calder | John Innis Centre | UK |
| Damir Sudar | Lawrence Berkeley National Laboratory | US |
| Felix Kraus | LMU Munich | DE |
| Katrin Schneider | LMU Munich | DE |
| Elke Küster-Schöck | McGill University | CA |
| Michael Cammer | New York University | US |
| Henrik Strahl von Schulten | Newcastle University | UK |
| Anil Shukla | NIH/NCI | US |
| Mariana Pinho | NOVA University of Lisbon | PT |
| Alison North | Rockefeller University | US |
| Monica Hasegan | Samuel Lunenfeld Research Institute | CA |
| Andrew Olson | Stanford University | US |
| John Mulholland | Stanford University | US |
| Manish Butte | Stanford University | US |
| Xiaoxue Zhou | Stanford University | US |
| Kathie Amberg-Johnson | UC Berkeley | US |
| Samantha Lewis | UC Davis | US |
| Stephen Ogg | University of Alberta | CA |
| Pascal Detampel | University of Calgary | CA |
| Alex Sossick | University of Cambridge | UK |
| Mark Bowen | University of Cambridge | UK |
| Nicola Lawrence | University of Cambridge | UK |
| Laure Plantard | University of Copenhagen | DK |
| Markus Posch | University of Dundee | UK |
| Peter Carlton | University of Kyoto | JP |
| Benjamin Hibbs | University of Melbourne | AU |
| Paul James McMillan | University of Melbourne | AU |
| Kay Oliver Schink | University of Oslo | NO |
| Richard Parton | University of Oxford | UK |
| George McNamara | University of Texas MD Anderson | US |
| Vito Mennella | University of Toronto | CA |

**SUPPLEMENTARY DATA**

Download:
https://www.dropbox.com/sh/4deho8b9cyjb8u7/AABWRZvfGu6M2B6hnmz_qLxxa?dl=0

**Supplementary Data 1** | OMX V3 Blaze example dataset 1. (**a**) Raw data and (**b**) reconstructed data (SIR) of a mouse C127 cell nucleus with chromatin stained with 4',6-diamidino-2-phenylindole (DAPI, blue, channel 1) and the proliferating cell nuclear antigen (PCNA) immuno-labelled with Alexa 488 (green, channel 2).

**Supplementary Data 2** | OMX V2 example dataset. (**a**) Raw data and (**b**) reconstructed data (SIR) of a HeLa cell in metaphase with $\alpha$-tubulin immuno-stained.

**Supplementary Data 3** | OMX V3 Blaze example dataset 2. (**a**) Raw data and (**b**) reconstructed data (SIR) of a dense layer of green fluorescent 100 nm diameter beads (505/515 FluoSpheres, Life Technologies).

**Supplementary Data 4** | Zeiss Elyra example dataset. (**a**) Raw data and (**b**) reconstructed data (SIR) of a three-color labelled human tissue culture cell nucleus (courtesy of S. Tashiro).

**Supplementary Data 5** | Nikon N-SIM example dataset. (**a**) Raw data and (**b**) reconstructed data (SIR) of a three-color labelled human liver cell section (courtesy of C. O'Connell).